Taylor & Francis
Taylor & Francis Group

Corrosion Engineering, Science and Technology

The International Journal of Corrosion Processes and Corrosion Control

ISSN: 1478-422X (Print) 1743-2782 (Online) Journal homepage: http://www.tandfonline.com/loi/ycst20

Modelling of radiolytic production of HNO_3 relevant to corrosion of a used fuel container in deep geologic repository environments

Ryan P. Morco, Jiju M. Joseph, David S. Hall, Chantal Medri, David W. Shoesmith & J. Clara Wren

To cite this article: Ryan P. Morco, Jiju M. Joseph, David S. Hall, Chantal Medri, David W. Shoesmith & J. Clara Wren (2017) Modelling of radiolytic production of HNO_3 relevant to corrosion of a used fuel container in deep geologic repository environments, Corrosion Engineering, Science and Technology, 52:sup1, 141-147, DOI: 10.1080/1478422X.2017.1340227

To link to this article: https://doi.org/10.1080/1478422X.2017.1340227

Published online: 23 Aug 2017.

CORROSION ENGINEERING, SCIENCE AND TECHNOLOGY, 2017
VOL. 52, NO. S1, 141–147
https://doi.org/10.1080/1478422X.2017.1340227

The Institute of Materials, Minerals and Mining

Taylor & Francis
Taylor & Francis Group

Modelling of radiolytic production of HNO_3 relevant to corrosion of a used fuel container in deep geologic repository environments

Ryan P. Morco [a], Jiju M. Joseph[a], David S. Hall [b], Chantal Medri [b], David W. Shoesmith[a,c] and J. Clara Wren[a]

[a]Department of Chemistry, The University of Western Ontario, London, ON, Canada; [b]Nuclear Waste Management Organization, Toronto, ON, Canada; [c]Surface Science Western, The University of Western Ontario, London, ON, Canada

ABSTRACT

Copper-coated steel containers are part of the engineered barrier system to permanently store Canadian nuclear fuel waste in a deep geological repository. This work models the dose rates (D_{Rs}) at the container surfaces as a function of fuel age. It also utilises a humid-air radiolysis model to study the effects of D_R and humidity on radiolytic oxidant production for conditions where unexpected early water intrusion reaches clay seal materials. Radiolysis of humid air produces HNO_3. The HNO_3 production rate in a condensed water droplet formed on a container surface was conservatively estimated by assuming that every •OH produced by primary radiolytic processes was immediately converted to HNO_3 in the gas phase and that all of the HNO_3 was absorbed in the water droplet. Also assuming that all of the nitric acid absorbed in the water droplet is consumed in corroding copper and using a hemispherical water droplet geometry, the corrosion depth of the copper coating induced by humid-air radiolysis is conservatively estimated to be 9.4 µm over the permanent storage time.

ARTICLE HISTORY
Received 16 January 2017
Accepted 5 May 2017

KEYWORDS
Humid-air radiolysis; nitric acid; radiolytic oxidants; kinetic model analysis; used fuel container dose rates

This paper is part of a supplement on the 6th International Workshop on Long-Term Prediction of Corrosion Damage in Nuclear Waste Systems.

Introduction

Canada's long-term plan for used nuclear fuel includes storage in a deep geological repository (DGR) using a multiple-barrier system [1]. A key barrier is the used fuel container (UFC), which was recently redesigned. The current UFC design consists of an inner vessel made of carbon steel (CS) for structural strength and an outer Cu coating as an external corrosion barrier [2]. Compared to the previous design, the CS vessel thickness is reduced considerably (from 10 to 4.6 cm) and the 25-mm-thick outer copper shell is replaced with a 3–4-mm thick integrally applied copper coating [1,2]. The use of a pressure-grade CS vessel and copper coating improves the mechanical integrity by eliminating many fabrication issues associated with the previous design. However, the possibility of localised CS corrosion near the weld region and the general corrosion of the copper coating of the new design must be assessed carefully to ensure the integrity of the inner vessel and the adequacy of the copper coating for corrosion protection.

Concerns arise about whether moisture trapped inside a UFC could condense on the internal surface, particularly near the CS weld regions. Corrosion within the gap between the hemispherical head and the body of the container assembly or in the stressed regions near the welds could lead to localised corrosion and potential failure of the container. The local environment (liquid water, water vapour, and humid air) and the UFC metal components will be exposed to the ionising radiation (particularly γ-radiation) emitted by decay of radionuclides in the used fuel. The radiation energy absorbed by metal is dissipated mainly as heat but it can induce ionisation and decomposition of water and gas-phase molecules to yield redox active species [3,4]. For example, γ-irradiation of water droplets would produce oxidants such as H_2O_2, while humid-air radiolysis would produce NO_x and HNO_3 that can dissolve in the water droplets. Since the thinner container design will provide less shielding for γ-radiation, the effect of γ-radiation on copper corrosion must be evaluated to ensure that the coating provides corrosion protection.

In this paper, the effects of radiation on container corrosion during long-term disposal in the anticipated DGR environments are evaluated. Model calculations are used to determine the concentrations of radiolytically produced oxidants that may potentially contact the container. The evolution of γ-radiation dose rates (D_{Rs}) with time for both internal and external surfaces of the current container design is calculated in the different aqueous environments (aerated and deaerated water, waters with impurity levels of solutes, saline water, water vapour) a container may experience under DGR conditions. This paper presents model calculations with a focus on the radiolytic production of HNO_3.

Dose rates at the internal and external surfaces of a UFC

In these calculations, only the γ-radiation from used Canada Deuterium Uranium fuel inside a container was considered since the emitted α- and β-particles will be adsorbed within the fuel and the fuel cladding and, hence, will not contribute to either internal or external surface D_{Rs}.

CONTACT J. Clara Wren jcwren@uwo.ca Department of Chemistry, The University of Western Ontario, London, ON, Canada N6A 5B7
Supplemental data for this article can be accessed https://doi.org/10.1080/1478422X.2017.1340227.

Table 1. Summary of internal and external UFC surface γ-radiation D_{Rs}.

Fuel age *a*	Internal surface[a] Gy h^{-1}	External surface Gy h^{-1}
10	5.1×10^{1}	2.3×10^{0}
20	3.4×10^{1}	1.4×10^{0}
30	2.5×10^{1}	1.1×10^{0}
50	1.6×10^{1}	6.4×10^{-1}
100	4.9×10^{0}	2.0×10^{-1}
200	4.8×10^{-1}	2.0×10^{-2}
500	1.7×10^{-3}	6.8×10^{-5}
1,000	1.2×10^{-3}	4.7×10^{-5}
10,000	1.2×10^{-3}	5.6×10^{-5}
100,000	1.9×10^{-3}	1.4×10^{-4}
1,000,000	2.6×10^{-3}	2.1×10^{-4}

[a]Includes assumed contribution from back-scattered β-radiation near the internal surface.
Fuel age refers to the time since the fuel was removed from the reactor.

Internal and external UFC surface γ-radiation D_{Rs} as a function of storage time were estimated for a base case involving used fuel with a burnup of 220 MWh kgU^{-1} using Microshield v9.05 and appropriate fluence to D_R conversion factors [5]. Because the software is not designed to model non-homogeneities in the shielding materials, the source was represented as a single cylinder of used fuel (UO_2) encapsulated in a layer of Zircaloy (modelled as zirconium) and the UFC was modelled as a layer of steel [6–8]. Moreover, MicroShield does not allow backscatter calculations (i.e. all dose points must be on the exterior of the modelled geometry). Therefore, the D_{Rs} on the internal surface of the container were modelled without the steel vessel and copper coating. As a conservative measure, these internal surface D_{Rs} were then multiplied by 1.3 to account for secondary electrons backscattering [9,10]. The full details of the radiation dose model, including the UFC and source geometries, with further details on the calculation assumptions and accuracy, and the results of three case that assess the sensitivity of the results to key assumptions, are provided in the supplementary information (SI-1). In general, the calculated D_{Rs} are very sensitive to the source parameterisation and should therefore be interpreted with an appropriate level of uncertainty.

The D_{Rs} calculated at the internal and external UFC surfaces, expressed as absorbed D_{Rs} in air, are presented in Table 1 and Figure 1. For the first 500 y, the γ-D_R is dominated by the decay of the fission products in the fuel and, hence, it decreases nearly exponentially with time. The D_R is subsequently dominated by the decay of the actinides present and decreases nearly linearly from 500 to 1,000,000 y. The accumulated dose on the container surfaces is also provided for reference, although there is no simple relationship between accumulated dose and the extent of corrosion damage in a changing radiation field as claimed elsewhere [11], see further discussion later. To approximate the accumulated dose on each surface, the D_R curves were fitted to mathematical functions (see supplementary information) and then integrated. The accumulated doses are shown in Figure 1.

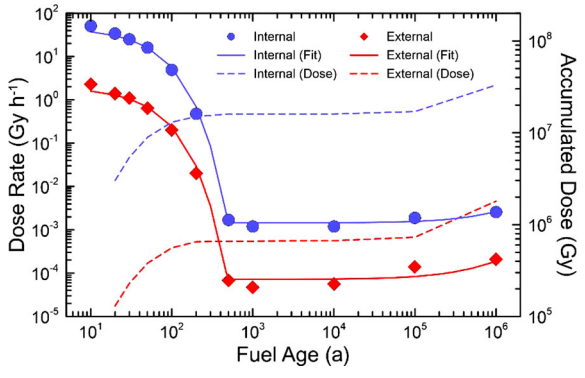

Figure 1. Calculated D_{Rs} and accumulated doses at the internal and external surfaces of the Canadian UFC, starting with 10-year-old fuel.

The D_{Rs} anticipated at the internal surface would be 20–25 times greater than those on the external surface of the container in the first 10,000 years and then only about 10 times greater thereafter, owing to the time-dependent change in the γ-radiation spectrum, as described above. The D_R to the external surface of a thin-walled container would decay from ~2.3 to ~0.02 Gy h^{-1} after 200 years. This is a significant (>20-fold) increase in the external fields compared to those anticipated in the previous thick-walled container [2].

Modelling approach for γ-radiolytic production of oxidants

The main objective of γ-radiolysis modelling is to determine the radiolytic oxidant concentrations that may affect the localised corrosion of the weld inside a UFC or the general/localised corrosion of the external copper coating. The initial environment inside a sealed UFC could be humid due to the combination of the ambient humidity of the air at the time of container sealing and that due to trapped water in the fuel bundles before encapsulation. For the localised corrosion of the CS weld region, γ-radiolysis of humid air and water droplets is the main concern. For the external copper coating, the DGR environment will evolve through a sequence of possible stages: (1) an initial aerated period with no condensed H_2O on the Cu surface, (2) a period of aerated vapour in equilibrium with a condensed H_2O layer on the surface, (3) a transition period to fully water-saturated air and potentially oxidising aqueous conditions, and (4) a final aqueous anoxic period after container corrosion and reactions with minerals and organic matter in the surrounding clay has consumed all of the available O_2 [2].

To address the different corrosion exposure environments, calculations using three different radiolysis kinetic models have been performed: (1) water radiolysis, (2) humid-air radiolysis, and (3) radiolysis of highly saline water. Each calculation determines the changes in radiolysis product concentrations ($[i]_t$) as a function of time by solving the rate equations of all the strongly coupled reactions that describe the chemistry of the environment. The processes that control the concentration of primary radiolysis product *i* under a continuous flux of radiation are as follows:

- the primary radiolysis process that produces *i*; and
- the chemical reactions of *i* with itself and other chemical species, *j*, including other radiolysis products, and dissolved chemical or reactive surface species present in the corresponding water phase.

The primary radiolysis processes that ionise and dissociate molecules act nearly instantly upon absorption of radiation energy [12–15]. This leads to radiolysis decomposition products uniformly distributed within an irradiated volume within ~100 ns following a radiation pulse input. The radiolysis products formed on this timescale are commonly referred to as primary radiolysis products whose chemical yields depend primarily on the total absorbed radiation

energy and hence the primary radiolysis product yields are expressed per unit of absorbed radiation energy and are commonly known as g-values in units of μmol·J^{-1}. Because the rate of radiation energy absorption by an interacting medium (D_R) depends primarily on the density of the medium, the D_R is typically expressed per unit mass in units of Gy (J kg^{-1})). For example, the g-values for liquid water radiolysis at room temperature (T) are given in brackets in reaction (R.1) [12,16]

$$H_2O(liq.) \overset{\gamma}{\rightsquigarrow} \bullet OH(0.26),\ \bullet e^-_{aq}(0.26),\ \bullet H(0.06),\ H_2(0.045),\ H_2O_2(0.075),\ H^+(0.26) \quad (R.1)$$

For the analysis of the radiolysis product concentrations on the timescale of corrosion reactions (>1 ms), modelling of the detailed kinetics of the radiolysis processes at very short timescales (<1 μs) is not necessary. Thus, the production rates of primary radiolysis products can be simplified to a rate proportional to its g-value (g_i), D_R, and the density of the medium, ρ_W

$$\text{primary production rate, } \frac{d[i]}{dt} = 10^{-6} \cdot g_i \cdot D_R \cdot \rho_w \quad (1)$$

where $[i]$ is the concentration of species, i, in units of M (mol dm^{-3}).

However, the primary radiolysis products are reactive and rapidly undergo chemical reactions with each other, with water and its acid and base ions, and with solute species, producing secondary radiolysis products (such as O_2, $\bullet O_2^-$ and $\bullet HO_2$). Owing to the long penetration depth of a typical γ-ray (~20 cm for a half reduction in intensity in liquid water), the radiolysis products are created uniformly within a reasonably large volume of water. A consequence is that the concentration of a reactive species in the bulk phase is determined by a combination of the rates of primary radiolysis production and the chemical reactions of the species in solution

$$\left.\frac{d[i]_t}{dt}\right|_{net} \approx 10^{-6} \cdot g_i \cdot D_R \cdot \rho_w - \left(\sum_j k_{ij} \cdot [j]_t\right) \cdot [i]_t \quad (2)$$

where k_{ij} represents the rate constant of the chemical reaction between species i and j. Note that for a primary radiolysis product, the rate of any secondary production of this species via chemical reactions is typically negligible compared to the rate of the primary radiolysis process. The complex chemical kinetics involving many chemical species with strongly coupled reactions are solved numerically using commercially available software.

Specific models and the model calculation results that address the γ-radiolysis kinetics of liquid water containing dissolved oxygen, nitrate/nitrate, organic compounds (e.g. methyl ethyl ketone) and dissolved ferrous ions at a concentration level below <0.01 M have been reported elsewhere [17–19]. This paper focuses on the HNO_3 production by humid-air radiolysis.

Nitric acid production by humid-air radiolysis

Homogeneous radiolytic production of HNO_3 in the gas phase

Humid-air radiolysis produces nitric acid [20–22]. The HNO_3 formed in the gas phase will be continually absorbed in the condensed water droplets in contact with the humid air. This will lower the pH of the water in the droplet and increase the concentration of nitrate, a potential oxidant for CS and copper. The homogeneous radiolytic production of HNO_3 in the gas phase (HNO_3(g)) is described first. The section 'Aqueous concentrations of HNO_3 in water droplets' describes how the production rate in the gas phase may be used to estimate the production rate of HNO_3 in a water droplet (HNO_3(aq)). The section 'Bounding estimates for corrosion extents by radiolytically produced HNO_3' describes how it may be used in obtaining the upper bounding estimate for the extent of corrosion that can occur due to the radiolytic production of HNO_3 over the disposal period, and how the radiolytic production rate of HNO_3 could be incorporated in a corrosion model are discussed.

To calculate the production rate of HNO_3(g) by humid-air radiolysis and its rate of accumulation in condensed water droplets, a humid-air radiolysis model (HARM) has been constructed. The model is primarily based on the reaction set initially reported by Matzing and later modified by others [23–25]. For humid-air radiolysis, the absorption of radiation energy by the three main components of air (N_2, O_2, and H_2O) results in the formation of a range of primary products that include electronically excited and ionised molecules, ions and free radicals [26].

$$N_2(g) \overset{\gamma}{\rightsquigarrow} N_2^+(g),\ N^+(g),\ e^-(g),\ N(g),\ N^*{}_2(g) \quad (R.2)$$

$$O_2(g) \overset{\gamma}{\rightsquigarrow} O_2^+(g),\ O^+(g),\ e^-(g),\ O(g),\ O_2{}^*(g) \quad (R.3)$$

$$H_2O(g) \overset{\gamma}{\rightsquigarrow} H_2O^+(g),\ H_2(g),\ O(g),\ OH(g),\ H(g),\ O^+(g),\ e^-(g),\ H^+(g),\ OH^+(g) \quad (R.4)$$

The current version of HARM consists of the primary radiolytic production processes and about 730 chemical reactions involving 25 primary radiolysis products and 95 secondary species.

The HARM model was used to calculate the radiolytic production rate of HNO_3 in the gas phase as a function of D_R, relative humidity (RH), and T. The calculation results obtained as a function of RH at 75°C and at D_R 1 Gy h^{-1} are presented in Figure 2. At a given T and D_R, the main radiolysis product of dry air (0% RH) is O_3(g) at very short irradiation times, but this changes to NO_2(g) at longer times. When water vapour is present (as little as 10% RH), the main products are •OH(g), $\bullet HO_2$(g) at very short times, and HNO_3(g) at longer times.

Detailed kinetic analysis of the modelling results suggests that the precursors for HNO_3(g) production are •OH(g) and NO_2(g), where NO_2(g) is a secondary product of the γ-radiolysis of air.

$$\bullet OH(g) + \bullet NO_2(g) \rightarrow\rightarrow HNO_3(g)\% \quad (R.5)$$

The computational calculation results show that at a given D_R and a given RH at T, the concentration of •OH(g) at times shorter than a second (or <10^{-3} h) increases linearly with time (i.e. the slope of the log [•OH(g)] vs. log t plot is 1.0). This linear increase in $[\bullet OH(g)]_t$ with time is expected, because the main process controlling $[\bullet OH(g)]_t$ at times shorter than 1 s is the primary radiolytic production

$$\frac{d[\bullet OH(g)]}{dt} \approx 10^{-6} \cdot g_{\bullet OH} \cdot D_R \cdot \rho_w \quad (3)$$

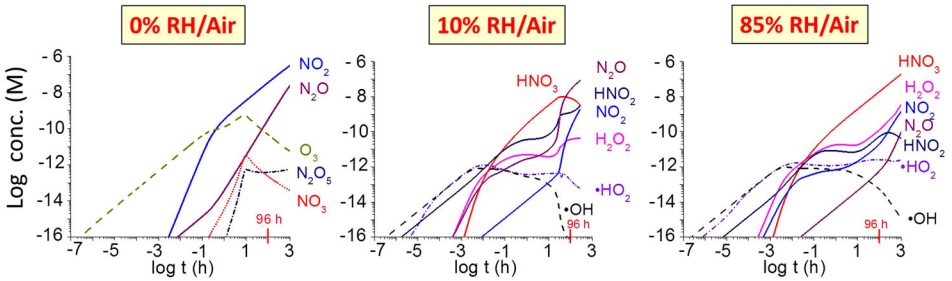

Figure 2. Time evolution of the concentrations of key radiolysis products formed during γ-radiolysis of 0, 10%, and 85% RH air at 75°C and a D_R of 1 Gy h^{-1}.

$$[\bullet OH(g)] \approx 10^{-6} \cdot g_{\bullet OH} \cdot D_R \cdot \rho_w \cdot t \quad (4)$$

The overall production rate for the secondary radiolysis product, $\bullet NO_2$, is initially slow, but rapidly increases and $[\bullet NO_2(g)]_t$ becomes comparable with those of other radiolysis products in 10^{-3} h or ~4 s. The rate of $\bullet NO_2(g)$ reaction with •OH(g) becomes significant and can compete with other •OH(g) reactions, particularly that of $H_2O_2(g)$. Note that $H_2O_2(g)$ is also a secondary product of humid-air radiolysis (formed by multi-step reactions of •OH(g) and $\bullet HO_2(g)$ [23–25]). When the concentrations of secondary products ($\bullet NO_2(g)$ and $H_2O_2(g)$) reach high levels, they can react with •OH(g) at substantial rates. The overall production rates of $H_2O_2(g)$ and $NO_2(g)$ slow down and that of •OH(g) becomes approximately zero. These kinetic progressions of $[\bullet OH(g)]_t$, $[H_2O_2(g)]_t$ and $[NO_2(g)]_t$ can be appreciated from Figure 2. As $[H_2O_2(g)]_t$ and $[NO_2(g)]_t$ reach about 10^{-13} M, $[\bullet OH(g)]_t$ starts to deviate from the linear dependence on time and reaches near steady state.

The full model calculation results (Figure 2) show that the overall production rate for $HNO_3(g)$ at times longer than a minute is mainly determined by the primary radiolytic production of •OH(g) and the competition rates for •OH(g) between $\bullet NO_2(g)$ and $H_2O_2(g)$. That is, the overall radiolytic production of $HNO_3(g)$ at times longer than a minute can be approximated as

$$\frac{d[HNO_3(g)]_t}{dt} \approx f_{NO_2-OH} \cdot \frac{d[\bullet OH(g)]_t}{dt} \quad (5)$$

$$\frac{d[HNO_3(g)]_t}{dt} \approx f_{NO_2-OH} \cdot 10^{-6} \cdot g_{\bullet OH(g)} \cdot D_R \cdot \rho_w \quad (6)$$

$$f_{NO_2-OH} \approx \frac{k_{NO_2-OH} \cdot [NO_2]_t}{\left(\sum_j k_{j-OH} \cdot [j]_t\right)} \approx \frac{k_{NO_2-OH} \cdot [NO_2]_t}{k_{NO_2-OH} \cdot [NO_2]_t + k_{H_2O_2-OH} \cdot [H_2O_2]_t} \quad (7)$$

for t > 1min

where f_{NO_2-OH} is the fraction of •OH(g) reactions leading to the formation of $HNO_3(g)$, and k_{j-OH} represents the rate constant of the chemical reaction between species j and •OH(g).

The fraction, f_{NO_2-OH}, changes rapidly with time at early times, but the change becomes much slower. Thus, for a given D_R, RH, and T, Equation (7) shows that the overall production rate of $[HNO_3(g)]_t$ can be approximated as

$$[HNO_3(g)]_t \approx f_{NO_2-OH} \cdot 10^{-6} \cdot g_{\bullet OH(g)} \cdot D_R \cdot \rho_w \cdot t \quad (8)$$

Because of the competitions between the reactions of •OH(g) with $\bullet NO_2(g)$ and $H_2O_2(g)$, the overall production rate of $HNO_3(g)$ has a small dependence on RH at a given T and D_R. The model calculations performed as a function of RH at 75°C show that the f_{NO_2-OH} at times longer than 1 min is nearly one at 10% RH. As the humidity level ($[H_2O(g)]$) increases while the concentrations of air molecules ($[N_2(g)]$ and $[O_2(g)]$) remain constant, the primary radiolytic production of •OH(g) increases due to an increase in ρ_w. However, the production of $H_2O_2(g)$ also increases due to higher production of •OH(g) and $\bullet HO_2(g)$ (via $\bullet H + O_2$). On the other hand, $[H_2O(g)]$ has a negligible effect on $\bullet NO_2(g)$ production.

The overall effect of RH on $f_{NO_2-OH} \cdot \rho_w$ at times >1 min is thus relatively small. The plot of log $[HNO_3(g)]_t$ vs. log t (Figure 3) is shifted by log (½ RH), showing that the overall production rate of $HNO_3(g)$ decreases by about a factor of ½ RH.

Equation (8) shows that the overall production rate of $[HNO_3(g)]_t$ is proportional to D_R for a given RH and T which is consistent with computational modelling results. The time evolutions of $[HNO_3(g)]_t$ calculated for γ-radiolysis of 85% RH air at 75°C and different D_Rs (0.01 to 10 Gy h^{-1}) are compared in Figure 4. The computational modelling results show that the linear plot of log $[HNO_3(g)]_t$ vs. log t also shifts to a higher $[HNO_3(g)]_t$ proportionally to log (D_R), confirming the linear dependence of $[HNO_3(g)]_t$ on D_R as defined in Equation (8). That is, the rate of production of $HNO_3(g)$, and $[HNO_3(g)]_t$ at a given t, increase proportionally with D_R.

Aqueous concentrations of HNO_3 in water droplets

As noted earlier, the calculations presented in Figures 2 –4 do not take into account any adsorption or surface reactions involving the radiolysis products. Furthermore, the calculated concentrations are those in the gas phase. For the degradation of metal, aqueous corrosion is the main concern. Thus, for the corrosion of the CS inner vessel and the copper coating of the

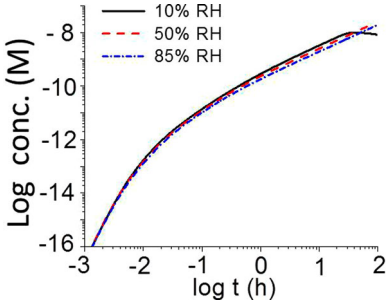

Figure 3. Time evolutions of $[HNO_3(g)]$ produced by γ-radiolysis of air for different RHs at 75°C and at D_R of 1 Gy h^{-1}.

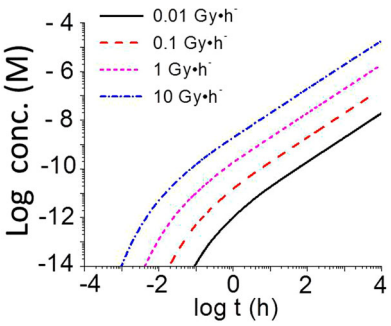

Figure 4. Time evolutions of [HNO_3(g)] produced by γ-radiolysis of 85% RH air at 75°C at different D_{Rs}.

container, the main concern is the HNO_3 that condenses in water droplets on the container surfaces which can then participate in the electrochemical reactions associated with aqueous corrosion. The water in the droplets will also be subject to radiolysis, but γ-radiolysis of liquid water does not produce HNO_3. Thus, the main route for the production of HNO_3(aq) in a water droplet in contact with humid air in the presence of continuous flux of γ-radiation is the deposition of HNO_3(g) formed in the gas phase by the humid-air radiolysis.

The accurate modelling of $[HNO_3(aq)]_t$ in water droplets will require solving the kinetics of liquid water radiolysis coupled with humid-air radiolysis via gas–liquid interfacial transfer of radiolysis products and its consumption due to corrosion. The accurate modelling of $[HNO_3(aq)]_t$ in the water droplets that may form on the Cu-coated container surface under the DGR conditions is futile and impractical because of an infinite combinations of water droplet and the headspace geometries. However, we can obtain the bounding estimates for $[HNO_3(aq)]_t$ in a water droplet to assess the corrosion behaviour of a waste container. This section explores these bounding estimates.

The production rate of $[HNO_3(aq)]_t$ in a water droplet is determined by the deposition rate of HNO_3(g) formed by humid-air radiolysis onto the water droplet surface. This deposition rate increases with $[HNO_3(g)]_t$. The maximum $[HNO_3(g)]_t$ can be achieved when the removal rate of HNO_3(g) by the gas-phase chemical reactions of HNO_3(g) is negligible, i.e.

$$k_{ad} \cdot [HNO_3(g)] > \left(\sum_j k_{ij} \cdot [j]_t\right) \cdot [HNO_3(g)]_t \quad (9)$$

The rate equation for $[HNO_3(g)]_t$ when the deposition rate becomes significant can then be approximated as

$$\frac{d[HNO_3(g)]_t}{dt} \approx f_{NO_2-OH} \cdot 10^{-6} \cdot g_{\bullet OH(g)} \cdot D_R \cdot \rho_w - k_{ad} \cdot [HNO_3(g)]_t \quad (10)$$

$$k_{ad} = v_{ad} \cdot \left(\frac{A_{aq-g}}{V_g}\right) \quad (11)$$

where k_{ad} represents the first-order adsorption rate constant in unit of s^{-1} and it depends on the ratio of water–gas interfacial surface area (A_{aq-g}) to gas volume (V_g). Owing to the near infinite solubility of HNO_3 in water, the deposition velocity (v_{ad}) is expected to be constant with time. However, the water droplet may grow with time and, hence, A_{aq-g} and V_g may vary with time.

The corresponding rate equation for $[HNO_3(aq)]_t$, when the aqueous-phase and surface reactions of HNO_3(aq) is negligible, is

$$\frac{V_{aq}}{V_g} \cdot \frac{d[HNO_3(aq)]_t}{dt} \approx k_{ad} \cdot [HNO_3(g)]_t \quad (12)$$

where V_{aq} represents the water droplet volume. Equation (10) shows that the maximum HNO_3(g) deposition rate that can be achieved is the rate of radiolytic production of HNO_3(g), i.e.

$$k_{ad} \cdot [HNO_3(g)]_t \approx f_{NO_2-OH} \cdot 10^{-6} \cdot g_{\bullet OH(g)} \cdot D_R \cdot \rho_w \quad (13)$$

The maximum production rate for $[HNO_3(aq)]_t$ in a water droplet is then further simplified to

$$\frac{d[HNO_3(aq)]_t}{dt} \approx \frac{V_g}{V_{aq}} \cdot f_{NO_2-OH} \cdot 10^{-6} \cdot g_{\bullet OH(g)} \cdot D_R \cdot \rho_w \quad (14)$$

Assuming D_R and RH change at much slower rates than $[HNO_3(aq)]_t$ does

$$[HNO_3(aq)]_t \approx \frac{V_g}{V_{aq}} \cdot f_{NO_2-OH} \cdot 10^{-6} \cdot g_{\bullet OH(g)} \cdot D_R \cdot \rho_w \cdot t \quad (15)$$

Thus, at a given D_R, RH, and T, $[HNO_3(aq)]_t$ in a water droplet will increase proportionally with the ratio of gas volume to water droplet volume. Note that f_{NO_2-OH} depends on D_R.

The current version of HARM calculates that the production rate of HNO_3(g) in the gas phase at 85% RH and 75°C would be about 2.0×10^{-10} M h^{-1} at a D_R of 1 Gy h^{-1}. To determine the corresponding production rate of HNO_3(aq) in a water droplet, we need to determine the effective ratio of V_g/V_{aq}. This ratio is estimated to be 100 based on the different diffusion coefficients of a compound in the gas and solution phases. The diffusion coefficient of a compound in the gas phase (D_g) is about 10,000 times greater than that in the solution phase (D_{aq}) [27]. Because HNO_3 can adsorb on any surface equally easily, the diffusion of HNO_3 from the gas phase to the container surface would be one dimensional. The ratio of one-dimensional diffusion length ($\propto\sqrt{D}$) in the gas phase to that in the water droplet is 100.

For the volume ratio of air to a droplet of 100, this results in a $[HNO_3(aq)]_t$ production rate in the water droplet of about 2.0×10^{-8} M h^{-1}. If $[HNO_3(aq)]_t$ continues to accumulate at this rate (without being consumed), the $[HNO_3(aq)]_t$ in the water droplet could reach up to about 0.5 μM in a day, 0.18 mM in a year or 18 mM in 100 years at a constant D_R of 1 Gy h^{-1}. The D_R at the external surface of the container is calculated to decrease from 2.3 to 0.2 Gy h^{-1} in 100 years (Figure 1). After 100 years, the D_R decreases more rapidly and decreases to a value below 0.1 mGy h^{-1} in 400 years, and the radiolytic production of HNO_3(aq) after 100 years would be significantly less. The simple analysis suggests that the $[HNO_3(aq)]_\infty$ that would accumulate over the full waste disposal period would be less than 100 mM, assuming that all of the HNO_3(g) produced radiolytically within a gas volume 100 times larger than the volume of a water droplet is absorbed in the water droplet.

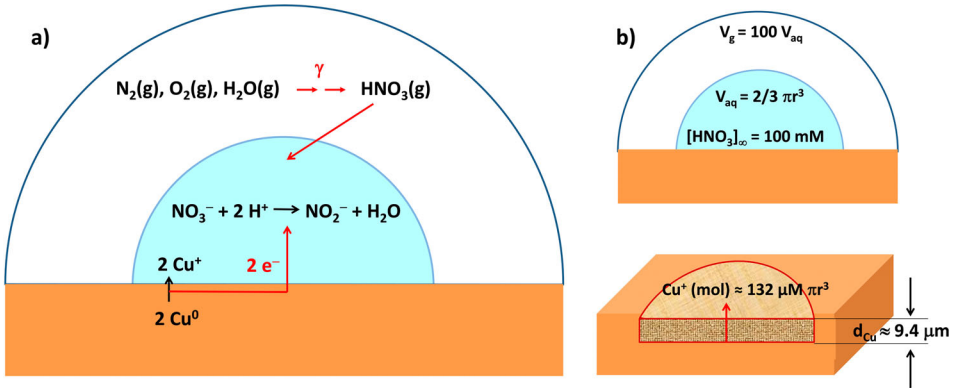

Figure 5. Schematics of (a) radiolytic and overall corrosion reactions, and (b) geometric parameters used in calculating corrosion depth.

Bounding estimates for corrosion extents by radiolytically produced HNO_3

The rate of metal corrosion depends on many environmental parameters including the solution pH, T, and redox conditions. The rate of corrosion also tends to evolve with time, even under constant exposure conditions, because the metal surface changes as corrosion progresses. Efforts are under way to develop detailed models of the corrosion of the container materials, although the present use of these models to predict an exact corrosion allowance would be premature. However, the upper limit for the extent of copper corrosion due to radiolytically produced HNO_3 can be estimated. Corrosion of copper produces two possible copper cations

$$2\ Cu^0 + NO_3^- + 2H^+ \rightarrow 2\ Cu^+(aq) + H_2O + NO_2^- \rightarrow Cu_2O(s) + NO_2^- + 2H^+\% \quad (R.6)$$

$$Cu^0 + NO_3^- + 2H^+ \rightarrow Cu^{2+}(aq) + H_2O + NO_2^-\% \quad (R.7)$$

The maximum concentration of dissolved metal ions in the water droplet would occur if corrosion resulted exclusively in the formation of Cu^+ (R.6). This concentration would be twice the $[HNO_3(aq)]_t$ accumulated in the water droplet if $HNO_3(aq)$ did not undergo any solution or corrosion reactions.

Assuming the volume ratio of air to droplet is about 100, the maximum cumulative nitric acid concentration over the permanent disposal period, $[HNO_{3(aq)}]_\infty$, would be less than 100 mM. Using this concentration and a hemispherical droplet geometry illustrated in Figure 5, the upper limit to the depth of copper corrosion, d_{Cu}, can be calculated as follows:

$$d_{Cu} = \frac{M_{Cu} \cdot 2\ [HNO_3(aq)]_\infty \cdot V_{aq}}{\rho_{Cu} \cdot A_{int}} \quad (16)$$

where M_{Cu} is the atomic mass of Cu (63.55 g mol^{-1}), ρ_{Cu} is the density of copper metal (8.96 g cm^{-3}), and A_{int} is the interfacial surface area covered by a droplet.

For a droplet with a radius of 1 cm and the $[HNO_{3(aq)}]_\infty$ of 100 mM, the depth of copper corrosion by radiolytically produced HNO_3 over the permanent disposal period would be

$$d_{Cu} \approx 9.4\ \mu m \quad (17)$$

This value was obtained assuming that all of the $HNO_3(g)$ produced radiolytically within a gas volume 100 times larger than the volume of a water droplet is absorbed in the droplet. For a given volume ratio, the corrosion depth would increase with water droplet radius. If the air volume is fixed, the $[HNO_3(aq)]_\infty$ would increase with decreasing water droplet radius. However, decreasing the water droplet radius also decreases the water droplet volume. The net effect of water droplet radius, r, on corrosion depth is that d_{Cu} is inversely proportional to r^2.

It is often suggested that the extent of corrosion damage depends on accumulated dose and not on D_R [11]. There are cases in which the overall corrosion may be determined by accumulated dose rather than D_R but that is more of a coincidence than fundamentally determined. Any chemical or electrochemical reaction rate depends on the concentration of a reactant and not on the total amount of the reactant introduced into the reaction system over the entire reaction time. For chemical or electrochemical reactions (such as corrosion) induced by radiation, accumulated dose is not a fundamental parameter [16]. The concept that total dose rather than D_R determines the effect of radiation on any chemical processes is only applicable for very short irradiation times when bulk phase chemical reactions of radiolysis products are not occurring at any substantial rates.

It has been also suggested that it is •OH and not HNO_3 that is the dominant species that causes copper corrosion in the presence of radiation [28]. The mechanism by which humid-air radiolysis affects copper corrosion requires in-depth discussion that is beyond the scope of this paper. Irrespective of whether •OH or HNO_3 is the dominant species driving corrosion, the estimate that we obtained for corrosion depth should still be bounding because it assumes that every •OH produced by the primary radiolysis process would eventually produce HNO_3 and that all of the HNO_3 produced that way would be consumed in corroding copper. However, it should be emphasised that the corrosion estimate does not take into account any radiolysis of water droplets. Radiolysis of liquid water produces H_2O_2 and O_2 that will more effectively contribute to copper corrosion than •OH.

Conclusions

The γ-radiation D_{Rs} at the internal and external surfaces of a Canadian copper-coated UFC were calculated using MicroShieldv9.05. As the used fuel ages from 10 to 10^6 a, the internal and external surface D_{Rs} decay from 51 to 2.6 mGy h^{-1} and from 2.3 to 0.21 mGy h^{-1}, respectively. Radiolysis of dry air initially produces $O_{3(g)}$ and later $NO_{x(g)}$

at longer irradiation times. In humid air, radiolysis produces initially •OH which can then react with air molecules and their decomposition products to produce nitric acid. The RH (10–80%) has no significant effect on the rate of HNO_3 production. The HNO_3 production rate in a condensed water droplet formed on a container surface was conservatively estimated by assuming that every •OH produced by primary radiolytic processes was immediately converted to HNO_3 in the gas phase and that all of the HNO_3 was absorbed in the water droplet. Also assuming that all of the HNO_3 absorbed in the water droplet is consumed in corroding copper and using a hemispherical water droplet geometry, the corrosion depth of the copper coating induced by humid-air radiolysis is conservatively estimated to be 9.4 μm over the permanent storage time.

Disclosure statement

No potential conflict of interest was reported by the authors.

Funding

This research is funded by a Collaborative Research and Development grant supported by NSERC and the Nuclear Waste Management Organization (NWMO).

ORCID

Ryan P. Morco http://orcid.org/0000-0003-0693-4691
David S. Hall http://orcid.org/0000-0001-9632-0399
Chantal Medri http://orcid.org/0000-0002-3001-3588

References

[1] NWMO. Implementing adaptive phase management 2016–2020. Toronto, Canada: Nuclear Waste Management Organization; 2015.
[2] Boyle CH, Meguid SA, et al. Mechanical performance of integrally bonded copper coatings for the long term disposal of used nuclear fuel. Nucl Eng Des. 2015;293:403–412.
[3] Joseph JM, Choi BS, Yakabuskie P, et al. A combined experimental and model analysis on the effect of pH and O2(aq) on gamma-radiolytically produced H2 and H2O2. Radiat Phys Chem. 2008;77:1009–1020.
[4] Yakabuskie PA, Joseph JM, Wren JC. The effect of interfacial mass transfer on steady-state water radiolysis. Radiat Phys Chem. 2010;79:777–785.
[5] ICRP. Conversion coefficients for use in radiological protection against external radiation, ICRP publication 74. Ann ICRP. 1996;26:3–4.
[6] Tait JC, Roman H, Morrison CA. Characteristics and radionuclide inventories of used fuel from OPG nuclear generating stations. Volume 1 – Main report, OPG 06819-REP-01200-10029-R00 Vol. 1. Toronto, Canada: Ontario Power Generation; 2000.
[7] Tait JC, Roman H, Morrison CA. Characteristics and radionuclide inventories of used fuel from OPG nuclear generating stations. Volume 2 – Radionuclide inventory data, OPG 06819-REP-01200-10029-R00 Vol. 2. Toronto, Canada: Ontario Power Generation; 2000.
[8] Tait JC, Hanna S. Characteristics and radionuclide inventories of used fuel from OPG nuclear generating stations. Volume 3 – Radionuclide inventory data decay times 10 to 300 years, OPG 06819-REP-01200-10029-R00 Vol. Toronto, Canada: Ontario Power Generation; 2001.
[9] Das IJ, Kahn FM. Backscatter dose perturbation at high atomic-number interfaces in megavoltage photon beams. Med Phys. 1989;16:367–375.
[10] Scrimger JW. Backscatter from high atomic number materials in high-energy photon beams. Radiology. 1977;124:815–817.
[11] Bjorkbacka A, Hosseinpour S, Johnson M, et al. Radiation induced corrosion of copper for spent nuclear fuel storage. Radiat Phys Chem. 2013;92:80–86.
[12] Spinks JWT, Woods RJ. An introduction to radiation chemistry. New York: Wiley-InterScience; 1990.
[13] Draganic IG, Draganic ZD. The radiation chemistry of water. New York: Academic Press; 1971.
[14] Farhataziz, Rodgers MAJ. Radiation chemistry: principles and applications. New York: VCH Publishers; 1987.
[15] Allen AO. The radiation chemistry of water and aqueous solutions. New York: Van Nostrand; 1961.
[16] Wren JC. Steady-state radiolysis: effects of dissolved additives. In: Wai CM, Mincher BJ, editors. ACS symposium series: nuclear energy and the environment. Washington (DC): American Chemical Society; 2010. p. 271.
[17] Yakabuskie PA, Joseph JM, Stuart CR, et al. Long-term gamma-radiolysis kinetics of NO_3^- and NO_2^-solutions. J Phys Chem A. 2011;115:4270–4278.
[18] Wren JC, Glowa GA. A simplified kinetic model for the degradation of 2-butanone in aerated aqueous solutions under steady-state gamma-radiolysis. Radiat Phys Chem. 2000;58:341–356.
[19] Driver P, Glowa G, Wren JC. Steady-state gamma-radiolysis of aqueous methyl ethyl ketone (2-butanone) under postulated nuclear reactor accident conditions. Radiat Phys Chem. 2000;57:37–51.
[20] Johnson GRA. The radiation chemistry of nitrogen and its compounds. Inorganic and theoretical chemistry. New York: Wiley; 1967.
[21] Sato S, Steinberg M. Radiation chemical nitrogen fixation in air-water systems, Report BNL-13652. New York: Brookhaven National Laboratory; 1969.
[22] Wittman R. Radiolysis model sensitivity analysis for used fuel storage canister, Report PNNL-22773. Richland, Washington: Pacific Northwest National Laboratory; 2013.
[23] Matzing H. Chemical-kinetics of flue-gas cleaning by irradiation with electrons. Adv Chem Phys. 1991;80:315–402.
[24] Willis C, Boyd AW, Young MJ. Radiolysis of air and nitrogen-oxygen mixtures with intense electron pulses – determination of a mechanism by comparison of measured and computed yields. Can J Chem. 1970;48:1515–1525.
[25] Schmitt KL, Murray DM, Dibble TS. Towards a consistent chemical kinetic model of electron beam irradiation of humid air. Plasma Chem Plasma P. 2009;29:347–362.
[26] Willis C, Boyd AW. Excitation in radiation-chemistry of inorganic gases. Int J Radiat Phys Chem. 1976;8:71–111.
[27] Lide DR, editor. CRC handbook of chemistry and physics. 89th ed.Boca Raton, FL: CRC Press/Taylor and Francis; 2009.
[28] Björkbacka Å, Johnson CM, Leygraf C, et al. Radiation induced corrosion of copper in humid air and argon atmospheres. J Electrochem Soc. 2017;164:C201–C206.